



**HAL**  
open science

## Spectroscopic characterization of black N- and P-doped zeolite templated carbons

Shuang Tan, Francesco Dalena, Igor Golub, Eddy Dib, Oleg Filippov, Ludovica Pace, Rémy Guillet-Nicolas, Valentin Valtchev, Hailing Guo, Svetlana Mintova

► **To cite this version:**

Shuang Tan, Francesco Dalena, Igor Golub, Eddy Dib, Oleg Filippov, et al.. Spectroscopic characterization of black N- and P-doped zeolite templated carbons. *Microporous and Mesoporous Materials*, 2025, 381, 10.1016/j.micromeso.2024.113347 . hal-04760400

**HAL Id: hal-04760400**

**<https://hal.science/hal-04760400v1>**

Submitted on 30 Oct 2024

**HAL** is a multi-disciplinary open access archive for the deposit and dissemination of scientific research documents, whether they are published or not. The documents may come from teaching and research institutions in France or abroad, or from public or private research centers.

L'archive ouverte pluridisciplinaire **HAL**, est destinée au dépôt et à la diffusion de documents scientifiques de niveau recherche, publiés ou non, émanant des établissements d'enseignement et de recherche français ou étrangers, des laboratoires publics ou privés.

## **Spectroscopic characterization of black N- and P-doped zeolite templated carbons**

*Shuang Tan<sup>1,2</sup>, Francesco Dalena<sup>2,\*</sup>, Igor E. Golub<sup>2</sup>, Eddy Dib<sup>2</sup>, Oleg A. Filippov<sup>3</sup>, Ludovica Pace<sup>2</sup>, Rémy Guillet-Nicolas<sup>2</sup>, Valentin Valtchev<sup>2</sup>, Hailing Guo<sup>1,\*</sup>, Svetlana Mintova<sup>2</sup>*

<sup>1</sup>China University of Petroleum, Qingdao 266580, China

<sup>2</sup>Normandie Univ, ENSICAEN, UNICAEN, CNRS, Laboratoire Catalyse et Spectrochimie, Caen, 14000, France

<sup>3</sup>A. N. Nesmeyanov Institute of Organoelement Compounds, Russian Academy of Sciences (INEOS RAS), 28, Vavilova St, Moscow, 119991, Russia

E-mail: [francesco.dalena@ensicaen.fr](mailto:francesco.dalena@ensicaen.fr), [guohl@upc.edu.cn](mailto:guohl@upc.edu.cn)

Keywords: Zeolite-templated carbon (ZTC), Nitrogen doped ZTC, Phosphorus doped ZTC, FTIR, NMR, DFT

The incorporation of heteroatoms (X) into the zeolite-templated carbon (ZTC) structure is a widely used technique to tailor its properties for specific applications such as gas adsorption, methane and hydrogen storage, and catalysis. However, the literature lacks sufficient data on Fourier-transform infrared spectroscopy (FTIR) analysis of ZTCs due to the challenge in obtaining high-quality FTIR spectra required for accurate assignment of the C–X bands, primarily caused by the black mass effect. In this work we prepared pure nitrogen (N) and phosphorus (P) doped ZTC samples using FAU type zeolite as a template and furfuryl alcohol as a carbon precursor. The FTIR spectra of the ZTC materials were obtained by controlling the preparation procedure and humidity, enabling clear analysis of the black samples. A Density Functional Theory (DFT) model based on the dimeric bucky bowl structure was developed and complemented by experimental results obtained from X-ray photoelectron spectroscopy (XPS), nuclear magnetic resonance (NMR), and FTIR. The proposed DFT model was then used for deconvolution and precise band assignment of the experimental FTIR spectra. The FTIR deconvolution study also supported the incorporation of N and P into the ZTC as well as the presence of primarily two types of nitrogen species, amide (primary and secondary) and pyridine-like, while P was mainly incorporated as triphenylphosphine oxide and phosphonic acid.

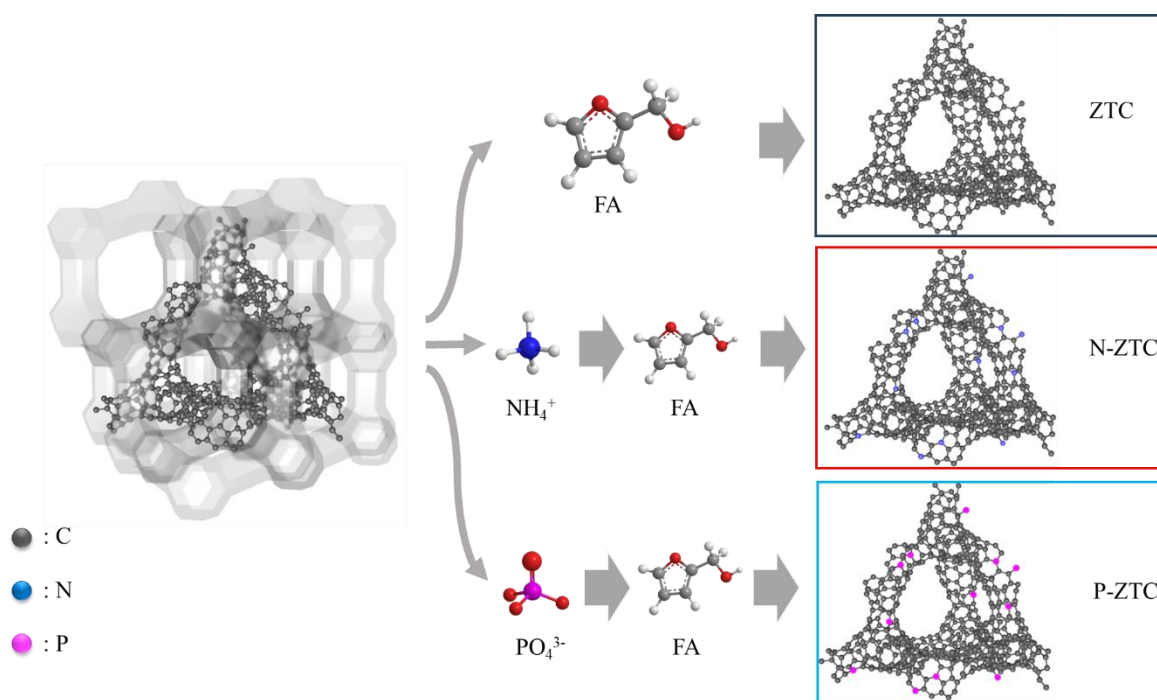
## 1. Introduction

Zeolite-Templated carbons (ZTCs) constitute a class of ordered microporous carbon materials that can be synthesized using large-pore zeolites such as beta (BEA) and faujasite (FAU) as templates.<sup>[1]</sup> As a result, the synthesized ZTCs are the negative replica of their porous structure templates and are therefore described by a 3D pore system with a uniform pore size distribution and high surface area, up to 4000 m<sup>2</sup>/g.<sup>[2]</sup>

The unique features of ZTCs make them attractive candidates for a variety of applications such as gas adsorption<sup>[3]</sup>, methane<sup>[4]</sup> and hydrogen storage<sup>[5]</sup>, and electrodes in capacitors and batteries.<sup>[6]</sup> Furthermore, the presence of oxygen, hydrogen and heteroatoms on the abundant edge sites can dramatically affect its reactivity.<sup>[7]</sup> From this one can consider to functionalize the ZTC with nitrogen<sup>[7]</sup>, boron<sup>[8]</sup> and sulfur<sup>[9]</sup> to enhance their affinity towards specific molecules for adsorption.

Two distinctive structural models have been proposed for ZTC produced using FAU as a sacrificial scaffold: (1) “closed-strut” schwarzite-like structure suggested by Roussel *et al.*<sup>[10]</sup> and (2) “open-blade” polyaromatic structure (Nishihara Model I), formed by interconnected bucky bowl-like subunits composed from carbon pentagons and hexagons, suggested by Nishihara *et al.*<sup>[11]</sup> These models have different compositions, functional groups on the edges, and carbon density per unit cell ( $g_{\text{carbon}}/g_{\text{zeolite}}$ ): 0.62–0.77 for “closed-strut” and 0.32–0.33 for “open-blade” structures. For this reason closed, schwarzite-like structures require more carbon per unit length and are characterized by a lower surface area (1440–1850 m<sup>2</sup>/g) compared to bucky bowl-like structures (3730–4790 m<sup>2</sup>/g).<sup>[12]</sup> However, most of the current models do not consider the presence of hydrogen (H/C ratio = 0.25)<sup>[13]</sup> and oxygen atoms (6–9 wt%)<sup>[10]</sup> on the edges. For example, the first schwarzite-like ZTC structure proposed by Roussel *et al.*<sup>[10]</sup> was a pure carbon model that was designed based on the experimental pore-size distribution without considering the chemical composition. However, Nishihara and co-workers<sup>[13]</sup> were the first to consider the real chemical composition of ZTC in their Model I (C<sub>75.3</sub>H<sub>19.0</sub>O<sub>5.7</sub> with H/C ratio = 0.25 and  $g_{\text{carbon}}/g_{\text{zeolite}}$  = 0.30). In the Model II, they proposed a H/C ratio of 0.38,  $g_{\text{carbon}}/g_{\text{zeolite}}$  of 0.3016 and considered irregularities and defects that were randomly generated using quenched molecular dynamics approach, while the Tanaka Model IV ( $g_{\text{carbon}}/g_{\text{zeolite}}$  = 0.32)<sup>[4]</sup>, considered higher disorder. However, with all these models it was impossible to experimentally reproduce a H/C ratio = 0.25 and/or experimental carbon density ( $g_{\text{carbon}}/g_{\text{zeolite}}$  = 0.29). Therefore, the development of new structural models that may better describe the experimental observables is an actual challenge.

Fourier-transform infrared spectroscopy (FTIR) and Raman spectroscopy are non-destructive methods which are used for the characterization of functional groups in carbon materials.<sup>[14]</sup> However, the determination of the nature and number of functional groups grafted onto the ZTC backbone has been challenging due to their high absorbance, and thus poor transmission. In addition, the non-uniform scattering of light makes it difficult to obtain useful IR spectra.<sup>[15]</sup> The electronic structure of carbon materials results in strong adsorption across the visible and infrared regions, limiting the collection of spectra in the conventional transmission mode. For these reasons, the obtained FTIR spectra of carbon-based materials exhibit unavoidable distortions, complicating their interpretation.<sup>[16]</sup> The initial FTIR spectra of ZTC materials prepared using furfuryl alcohol were first recorded by Nishihara *et al.*<sup>[11]</sup> These spectra revealed two distinct bands at 1720 and 1600  $\text{cm}^{-1}$ , along with two broad bands in the regions of 1400–1000  $\text{cm}^{-1}$  and 3400–3200  $\text{cm}^{-1}$ . This limited resolution can likely be attributed to a suboptimal signal-to-noise ratio, primarily due to the inherent absorbance characteristics of the analyzed black carbon. In this paper, we aim to optimize both the ZTC/KBr ratio and moisture levels to improve the quality of the FTIR spectra obtained for ZTC materials. The FTIR spectra of heteroatom-doped ZTC materials are also limited by the signal-to-noise ratio due to the proportion of heteroatoms in ZTC materials which is generally low. Furthermore the signals of heteroatom-containing bonds are obscured by the peaks of carbon-containing bonds. A crude FTIR spectrum on N-doped (with 4.8% of doping) ZTC materials was obtained; only traces attributed to C–N and N–H bonds were found.<sup>[17]</sup> In subsequent studies, other carbon-containing bonds, such as C–O–C and C=C, were observed in ZTC by FTIR spectroscopy.<sup>[18]</sup> It is important to note that the doping of certain heteroatoms has a large effect on the peak positions in the FTIR spectra of ZTCs. For example, after the treatment with sulfuric acid, most of the peaks were shifted.<sup>[18]</sup> Therefore, it is crucial to obtain FTIR spectra of ZTC of satisfactory quality to clearly distinguish different functional groups and thoroughly investigate the effects of heteroatoms on the spectra of ZTC materials. Herein, micron-sized zeolite templated carbon (ZTC), nitrogen-doped ZTC (N-ZTC), and phosphorous-doped ZTC (P-ZTC) were prepared and characterized with FTIR spectroscopy (Figure 1). The nature and the quantity of functional groups were confirmed by X-ray photoelectron spectroscopy (XPS) and nuclear magnetic resonance (NMR) spectroscopy to precisely assign the FTIR spectra. The deconvolution of the severely overlapped region in the FTIR spectra was performed, the accuracy of the deconvolution results was confirmed by both the experimental and the theoretical (DFT) results.

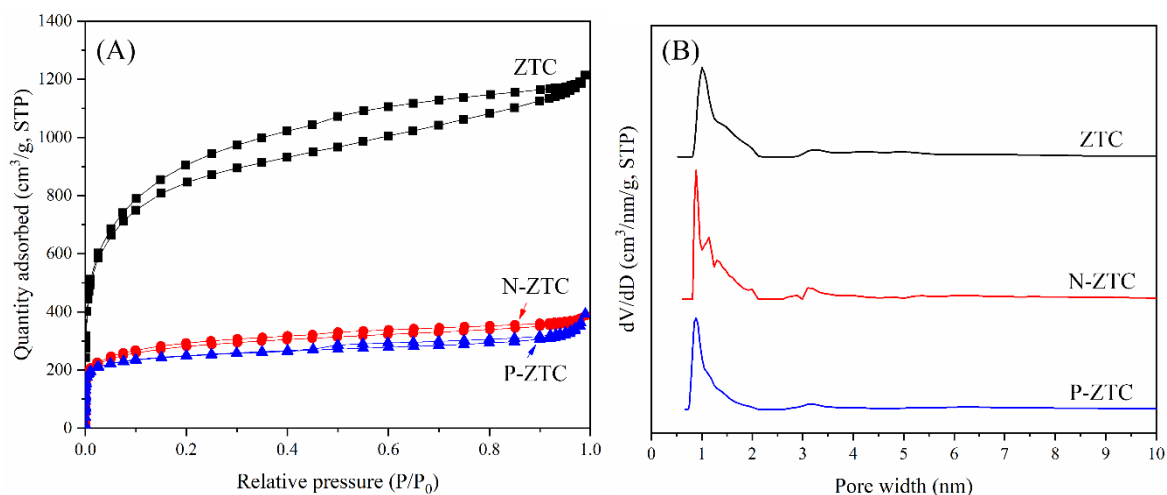


**Figure 1:** Schematic representation of the synthesis of the samples ZTC, N-ZTC, and P-ZTC

## 2. Result and discussion

### 2.1 General physicochemical characterization of ZTC, N-ZTC and P-ZTC samples

The three ZTC samples successfully replicated the FAU zeolite structure. The ZTC showed a crystalline peak ca.  $6.3^\circ 2\theta$  (Figure S3), which is an indicator of the long-range ordered crystalline FAU structure. The XRD patterns of samples N-ZTC and P-ZTC contain very low intensity peaks indicating low crystalline order. In addition, the three samples contain two broad Bragg peaks corresponding to C (0 0 2) and C (1 0 0) at  $25.0$  and  $43^\circ 2\theta$ . The presence of the heteroatom precursor catalysed the formation of poly-furfuryl alcohol, which cannot be removed by trimethylbenzene, and ultimately formed an external carbon layer during the calcination process. The textural properties of ZTC samples were characterized by  $N_2$  physisorption at  $-196^\circ C$ ; the results are shown in Figure 2 and Table 1.



**Figure 2:** N<sub>2</sub> sorption isotherms recorded at 77 K (A) and pore size distribution (B) of samples (a) ZTC, (b) N-ZTC, and (c) P-ZTC.

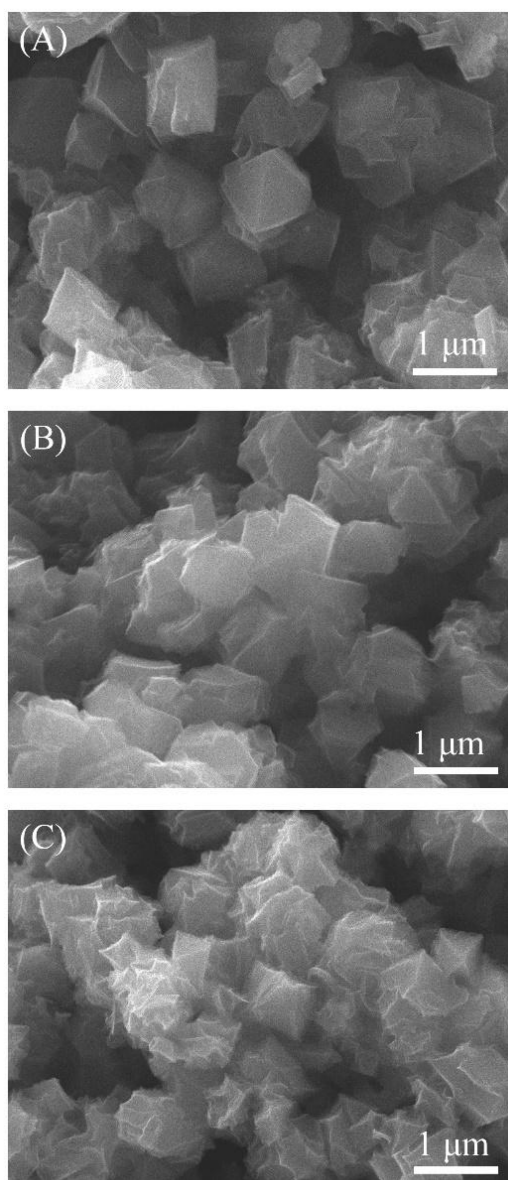
**Table 1:** Textural properties of ZTC, N-ZTC and P-ZTC samples

Sample name	$S_{\text{BET}}^{\text{a}}$ [m <sup>2</sup> /g]	$S_{\text{micro}}^{\text{b}}$ [m <sup>2</sup> /g]	$V_{\text{total}}^{\text{c}}$ [cm <sup>3</sup> /g]	$V_{\text{micro}}^{\text{d}}$ [cm <sup>3</sup> /g]
ZTC	2373	1937	1.747	0.973
N-ZTC	1031	900	0.522	0.359
P-ZTC	934	897	0.470	0.324

<sup>a)</sup> BET specific surface area calculated from the adsorption branch in  $P/P_0 = 0.02-0.15$ ; <sup>b)</sup> Micropore specific surface area calculated by the t-plot method; <sup>c)</sup> Total pore volume determined at  $P/P_0 = 0.97$ ; <sup>d)</sup> Micropore volume calculated from the v-t plot at  $P/P_0 = 0.4-0.6$ .

The high BET specific surface area of ZTC (2373 m<sup>2</sup>/g) indicates that the structure does not fit well to the schwarzite-like model (1440–1850 m<sup>2</sup>/g)<sup>[12]</sup> and the most probable one is rather the “open-blade” bucky bowl-like model. By adding the P- and N- precursors, the specific surface area and both micro- and total pore volumes of samples P-ZTC and N-ZTC decreased significantly, while the pore size of the three samples remains similar. The “low-pressure hysteresis” phenomenon observed in ZTC, as reported earlier, disappeared.<sup>[19]</sup> This phenomenon is attributed to the strong interactions between nitrogen molecules and the carbon skeleton, as documented in previous studies.<sup>[19-20]</sup> It is worth noting that this phenomenon has been reported in ZTC materials with large particle sizes, where mesoporosity was not observed.<sup>[21]</sup> Interestingly, the presence of this hysteresis disappears

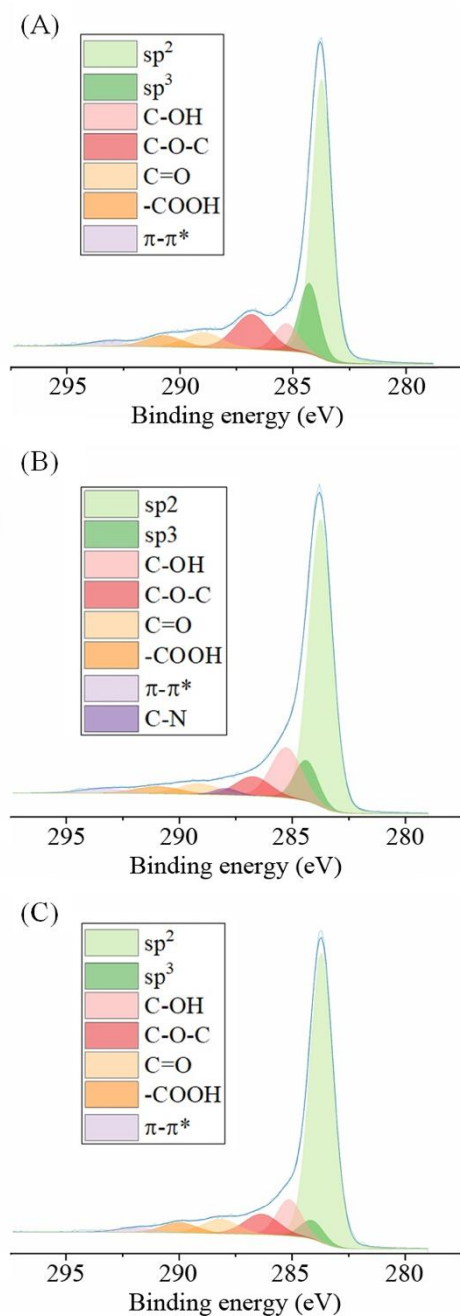
upon doping with heteroatoms. The introduction of heteroatoms may alter the strength of the interactions between the carbon skeleton and nitrogen molecules. This result showed the effect of the heteroatom precursors on the porosity of the ZTC structure. In addition to accelerating the formation of poly-furfuryl alcohol, the heteroatom precursors also occupied the space of the template zeolite channel, bringing more defects in the doped-ZTC structure. The SEM results, as presented in Figure 3, demonstrate the influence of the heteroatom doping on the ZTC samples. The ZTC samples exhibit a morphology similar to that of the zeolite template, characterized by well-defined octahedral-like shapes, which indicate a good replication of the zeolite structure and morphology. In contrast, the particle shapes of both N-ZTC and P-ZTC samples exhibit varying degrees of distortion. This distortion arises from the occupation of the pores by the precursors, leading to a less complete skeletal structure.<sup>[22]</sup>



**Figure 3.** SEM images of samples (A) ZTC, (B) N-ZTC, and (C) P-ZTC.

## 2.2 XPS and NMR spectroscopic characterization of ZTC, N-ZTC and P-ZTC samples

The ZTC, N-ZTC and P-ZTC samples were characterized by XPS. The C1s spectra (Figure 4) of the three samples contain at least six types of C species and their attribution, obtained by spectral deconvolution, are presented in Table 2.<sup>[23]</sup>



**Figure 4.** The C1s XPS spectra of samples (A) ZTC, (B) N-ZTC, and (C) P-ZTC.

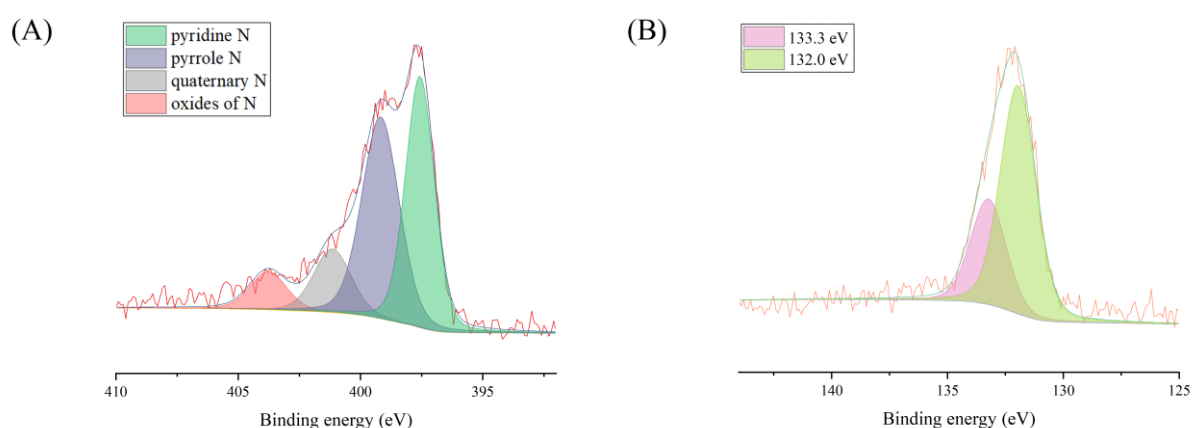


**Table 2.** Peak positions of the deconvoluted XPS spectra for samples ZTC, N-ZTC and P-ZTC.

	ZTC		N-ZTC		P-ZTC	
	Position	Ratio	Position	Ratio	Position	Ratio
	(eV)	(%)	(eV)	(%)	(eV)	(%)
$\pi$ - $\pi^*$	293.08	–	293.31	–	291.9	–
–COOH	290.71	4.29	290.95	3.08	289.99	3.71
C=O	288.93	5.71	289.15	3.91	288.17	5.18
C–N	–	–	287.93	1.51	–	–
C–O–C	286.81	12.67	286.74	6.17	286.34	7.37
C–OH	285.27	6.71	285.27	14.2	285.13	9.29
$sp^3$	284.27	14.69	284.38	8.92	284.11	4.57
$sp^2$	283.71	55.94	283.75	62.16	283.7	69.84
P–O	–	–	–	–	133.23	31.57
oxide of N	–	–	403.78	7.62	–	–
quaternary N	–	–	401.15	12.81	–	–
pyrrole N	–	–	399.18	40.58	–	–
pyridine N	–	–	397.57	38.99	–	–

The carbon  $sp^2$  ( $C\ sp^2$ ) is dominant, followed by carbon  $sp^3$  ( $C\ sp^3$ ), due to the graphene-like carbon structure of ZTC. The C1s spectrum also indicates several carbon species that are connected to O atoms by single or double bonds, which originates from the O atom in the furfuryl alcohol.

For sample N-ZTC (Figure 5), the N-containing functional group is present in the spectrum; a peak at 287.94 eV attributed to the C–N single bond is observed, while the peak of the C=N bond is overlapped by the  $C\ sp^2$ ,  $C\ sp^3$ , and C–OH peaks.<sup>[24]</sup>

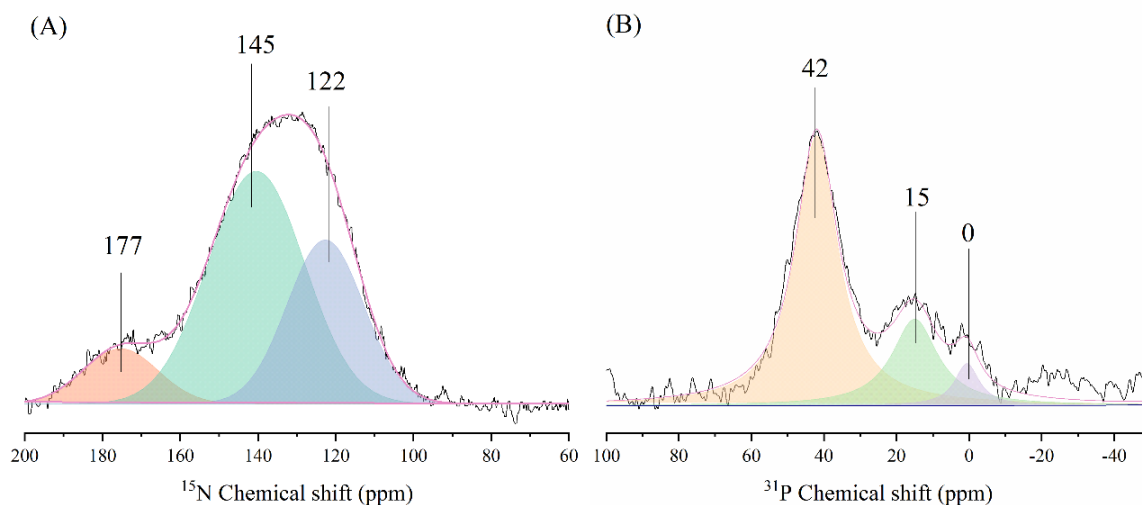


**Figure 5.** The N1s XPS spectrum of sample N-ZTC (A) and the P2p XPS spectrum of sample P-ZTC (B).

The existence of C=N functional groups in sample N-ZTC is verified by deconvolution of the N1s spectrum. The spectrum of the N-ZTC contains four types of N species, corresponding to the pyridine and pyrrole N domains. For the P-ZTC sample, by evaluating the binding energies of the P2p signal a single peak at 132.5 eV can be fit by two Gaussian functions at 133.0 and 132.0 eV which represent  $2p_{3/2}$  and  $2p_{1/2}$  of the oxidized phosphorus, respectively.<sup>[25]</sup>

The effect of N and P doping of ZTC was further evaluated by  $^{13}C$  (Figure S5),  $^{15}N$  (Figure 6A), and  $^{31}P$  NMR (Figure 6B) spectroscopy. The overall shifting of the band positions to a lower field when N is present, and slightly to a higher field in the presence of P, confirm the presence of C–N and C–P bonds, respectively. The  $^{15}N$  NMR spectrum of the sample N-ZTC contains a peak at 177 ppm that may be attributed to the existence of imide groups.<sup>[26]</sup> An additional broad peak at 130 ppm, deconvoluted into two peaks at 145 and 126 ppm, can be attributed to pyrrole N<sup>[27]</sup> and amide groups, respectively.<sup>[28]</sup> In the  $^{31}P$  MAS NMR spectrum of the sample P-ZTC, three bands at 42 ppm, 15 ppm, and 0 ppm corresponding to

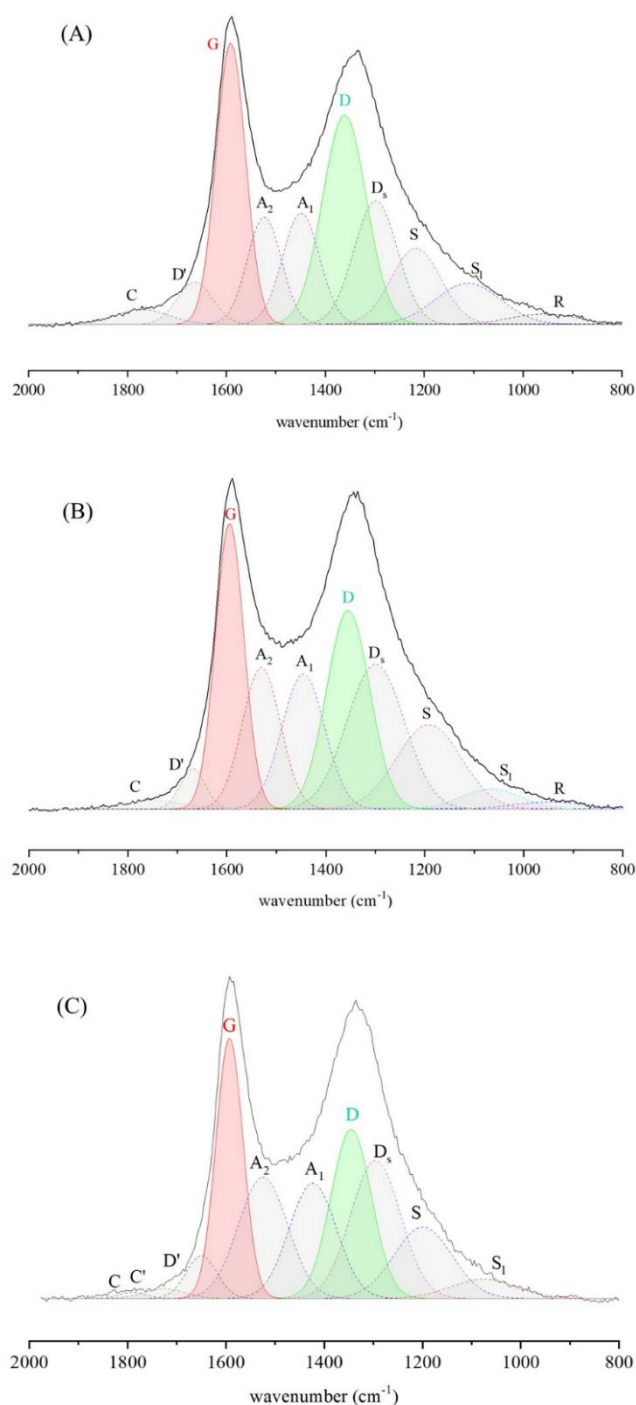
triarylphosphine oxide ( $\text{Ar}_3\text{P}=\text{O}$ ), arylphosphonic acid ( $\text{Ar}-\text{PO}(\text{OH})_2$ ), and aryl phosphate-like structures ( $\text{Ar}-\text{PO}_4$ ), respectively, are observed.<sup>[23]</sup>



**Figure 6.**  $^{15}\text{N}$  MAS NMR spectrum of N-ZTC (A) and  $^{31}\text{P}$  MAS NMR spectrum of P-ZTC (B).

### 2.3 Raman spectroscopic characterization of ZTC, N-ZTC and P-ZTC samples

Raman spectra of the samples recorded in the range of  $2000\text{--}800\text{ cm}^{-1}$  (Figure S4) were deconvoluted using a 10 Gaussian sub-peak method with (Figure 7).<sup>[29]</sup>



**Figure 7.** Deconvoluted Raman spectra of samples ZTC (A), N-ZTC (B) and P-ZTC (C).

The assignment of the Raman bands was done according to previously reported data (Table 3).<sup>[30]</sup> The D band was shown to be connected with a breathing mode in the  $C_6$  aromatic mode, and attributed to the  $C_6$  Kekulé vibrational modes.<sup>[31]</sup> The A1 band is related to  $C_5$  the breathing mode and could also be related to the  $C_6$  Kekulé vibrations. The frequencies of the D and A1 bands are decreased in samples N- and P-ZTC and correlates with the respective

atomic masses; this also proves the successful doping of the ZTC with N and P. The G band, in contrast to the D band, does not require presence of C<sub>6</sub> rings and is related to the stretching vibration >C=C< of C sp<sup>2</sup> in various polycyclic aromatic hydrocarbons (PAHs) and graphitic structures.<sup>[16]</sup> Tuinstra and Koenig<sup>[31]</sup> correlated the ratio of intensities of D and G bands (I<sub>D</sub>/I<sub>G</sub>) with the size of graphitic domains in carbonaceous materials. Therefore, the I<sub>D</sub>/I<sub>G</sub> ratio could be used to measure the degree of defects, bond-angle disorder, and amorphization of carbon materials.<sup>[25]</sup>

The I<sub>D</sub>/I<sub>G</sub> ratio of 1.0 for samples N-ZTC and P-ZTC slightly decreased compared to the parent ZTC (1.1) based on the Raman spectroscopic characterization. This result confirmed that the bulk ZTC structure is retained, however there are some structural defects due to the presence of N and P. According to previous reports, a decrease of the I<sub>D</sub>/I<sub>G</sub> ratio from 0.62 to 1.07 could indicate the presence of small- to medium-sized aromatic structures (up to C<sub>6</sub>), whereas an increase of I<sub>D</sub>/I<sub>G</sub> to 1.52 was proposed as threshold value for the presence larger aromatic structures (> C<sub>6</sub>).<sup>[29]</sup>

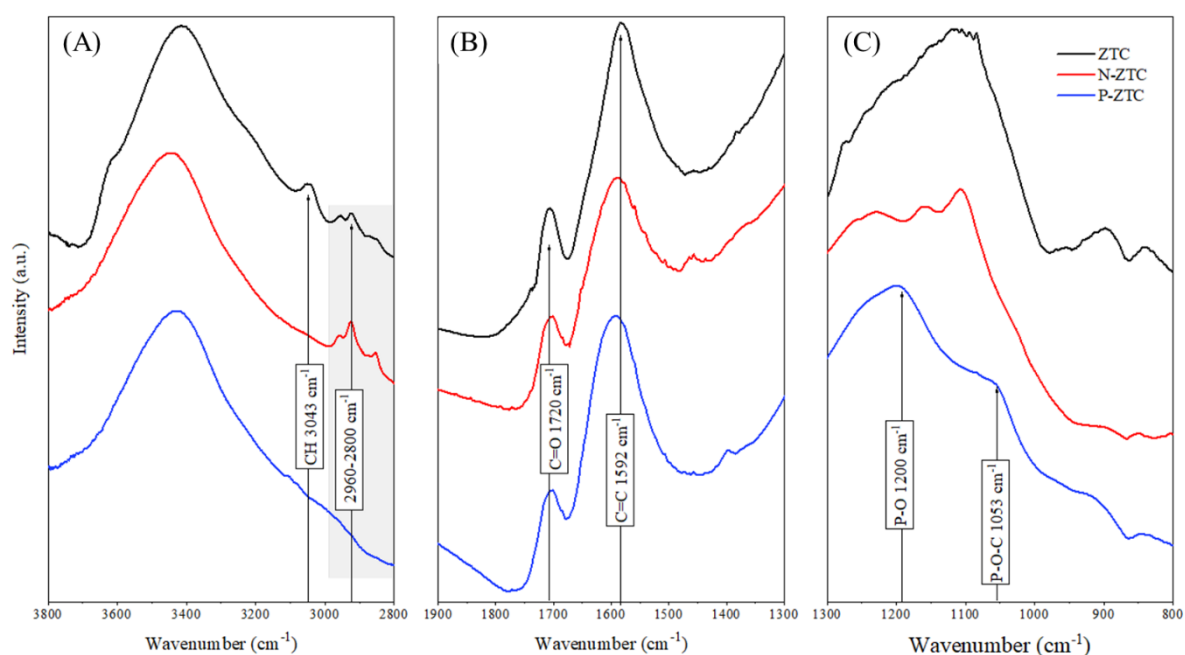
**Table 3.** Position and assignment of bands in the Raman spectra of samples ZTC, N-ZTC and P-ZTC.

ZTC [cm <sup>-1</sup> ]	N-ZTC [cm <sup>-1</sup> ]	P-ZTC [cm <sup>-1</sup> ]	$\nu_{\text{theoretical}}$ [cm <sup>-1</sup> ]	Band	Assignment
1771	1751	1790 1723	1800–1750	C/C <sup>*(a)</sup>	>C=O
1664	1668	1648	1650–1605	D <sup>(b)</sup>	Breathing mode
1593	1593	1593	1600–1570	G <sup>(c)</sup>	>C=C< of small PAH (E <sub>2g</sub> )
1522	1529	1525	1550–1480	A <sub>2</sub> <sup>(d)</sup>	C <sub>3</sub> -C <sub>5</sub> breathing C <sub>6</sub> Kekulé vibrations
1450	1446	1423	1460–1400	A <sub>1</sub> <sup>(d)</sup>	C <sub>5</sub> breathing C <sub>6</sub> Kekulé vibrations
1359	1356	1344	1380–1340	D <sup>(b)</sup>	C <sub>6</sub> Kekulé vibrations (A <sub>1g</sub> )
1296	1300	1296	1300–1250	D <sub>s</sub> <sup>(b)</sup>	Breathing mode of pyrene- like motifs
1217	1194	1197	1200–1150	S <sup>(e)</sup>	Breathing modes $\nu$ C–C, $\delta$ C–H

1111	1067	1075	1075–950	S <sub>i</sub> <sup>e)</sup>	Breathing modes benzene, naphthalene $\delta$ C–H
a) Carbonyl band; b) Defect bands; c) Graphitic bands;					
d) Amorphous bands; e) Shoulder band (low)					

## 2.4 FTIR spectroscopic characterization of ZTC, N-ZTC and P-ZTC samples

The FTIR spectra of each of the samples contain the characteristic bands in the range 3600–3400 cm<sup>-1</sup>, attributed to the O–H stretching vibrations (Figure 8a). The broad peak centred at 3450 cm<sup>-1</sup> originates primarily from the sum of phenolic hydroxyls, carboxylic acid, and intramolecular hydrogen bond adsorption.<sup>[32]</sup> More intense absorption bands in sample ZTC are observed. This is due to the higher relative concentrations of alcohol and carboxyl groups in the pure carbonaceous ZTC sample. The higher concentration of this specific functional group is likely associated with the surface area of the ZTC sample, which is approximately twice that of the other two samples.



**Figure 8.** FTIR spectra of samples ZTC (black), N-ZTC (red) and P-ZTC (blue) in the region 3800–2800 cm<sup>-1</sup> (A), 1900–1300 cm<sup>-1</sup> (B), 1300–800 cm<sup>-1</sup> (C).

The band at 3043 cm<sup>-1</sup> is related to the absorption of the coordinated CH groups on sp<sup>2</sup> hybridized carbons, while the bands in the range 2960–2800 cm<sup>-1</sup> are ascribed to the coordination of H on sp<sup>3</sup> hybridized carbons.<sup>[14]</sup> In particular, the spectra contain strong absorption bands at 2920 cm<sup>-1</sup> and 2850 cm<sup>-1</sup> corresponding to in-phase and out-of-phase

vibrations of the hydrogen atoms of CH<sub>2</sub> groups (hybridized sp<sup>3</sup>). At higher frequencies, two absorption bands at 2956 cm<sup>-1</sup> and 2866 cm<sup>-1</sup> are observed, corresponding to the asymmetric and symmetric stretching modes of CH<sub>3</sub> groups.<sup>[14]</sup> From the comparison of the three samples in the region 3800–2800 cm<sup>-1</sup> of the spectra, the following aspects are highlighted: the N-ZTC sample shows a clear major absorption band in the C–H stretching region of the sp<sup>3</sup> hybridized carbon, while the contribution of carbon in samples P-ZTC decreases. The difference between the samples is derived from an alteration of the aliphatic chain spacer (CH<sub>2</sub>CH<sub>2</sub>) connecting the semi-spheres of buckyball in the ZTC structure. Indeed, the intensities of the CH<sub>2</sub> and CH<sub>3</sub> bands are directly related to the amount of these groups present and the intensities of the CH<sub>2</sub> bands change by a steady increment for each unit increase in chain length.<sup>[33]</sup>

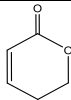
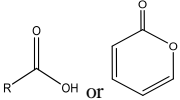
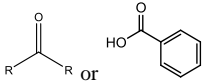
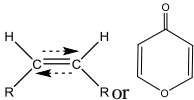
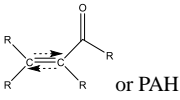
In addition, the absence of peaks at lower frequencies in the region 2825–2780 cm<sup>-1</sup> suggests that the nitrogen present in the structure is not coordinated with methyl groups, either in mono-substituted or di-substituted species (CH<sub>3</sub>N= or (CH<sub>3</sub>)<sub>2</sub>N-).<sup>[33]</sup> In fact, the potential presence of nitrogen directly linked to the methyl group causes the shift of the absorption C–H band to lower frequencies due to the Fermi resonance interaction.<sup>[34]</sup> Furthermore, for the N-ZTC and P-ZTC samples, a net decrease in the C–H stretching of the sp<sup>2</sup> hybridized carbon is observed. This is possibly a consequence of a decreased amount of non-conjugated >C=C< species due to the presence of defects in the later samples.

The FTIR spectra of the dehydrated samples (1900–1300 cm<sup>-1</sup> region) contain two peaks, in the regions 1740–1705 cm<sup>-1</sup> and 1660–1590 cm<sup>-1</sup>, representing the stretching vibrations of >C=O and >C=C< sp<sup>2</sup> bonds, respectively. In the region 1730–1700 cm<sup>-1</sup>, an overlapping contribution of carbonyl stretching bands at 1739, 1721 and 1707 cm<sup>-1</sup> in the ZTC sample is observed.<sup>[34]</sup> The band at 1721 cm<sup>-1</sup> can be attributed to carboxylic acids for black carbon materials,<sup>[35]</sup> or could also be assigned to the presence of the 2-pyrone motif in the structure.<sup>[36]</sup> In addition, the band at 1707 cm<sup>-1</sup> can have a double attribution. In fact, this band is mainly attributed to the presence of ketone groups, however, some studies have shown that this band can be also related to ν (>C=O) α,β-unsaturated carboxylic acids (1705–1690 cm<sup>-1</sup>) and also to the aryl acids (1700–1680 cm<sup>-1</sup>).<sup>[33]</sup> In the study of the use of FTIR analysis on activated carbon, it was reported that the presence of 2-pyrone (1740–1706 cm<sup>-1</sup>) or 4-pyrone (1688–1650 cm<sup>-1</sup>) motifs in the structure may be evidenced by the stretching band at 1720 cm<sup>-1</sup> along with the band at 1657 cm<sup>-1</sup>.<sup>[36]</sup>

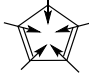
In the region of the stretching of >C=C< olefinic vibrations (1592 cm<sup>-1</sup>), a clear shift (Δν = 7 cm<sup>-1</sup>) for the N-ZTC and P-ZTC samples is observed, compared to the ZTC sample (Figure 8

(b)). The peak centred at  $1592\text{ cm}^{-1}$  is a sum of an overlapping of several bands related to the  $>\text{C}=\text{C}<$  stretching. However, the presence of an adsorption band at a specific frequency in the specific region of stretching of the  $>\text{C}=\text{C}<$  group cannot by itself be taken as evidence of the presence of a certain type of double bond. On the other hand, examining all functions in regions where specific adsorption frequencies occur may allow for a certain identification of the double bond and its type. For this reason, a deconvolution of the peaks present in the  $1750\text{--}1500\text{ cm}^{-1}$  region of the spectrum has been performed (Figure 9). The peaks and their attributions are summarized in Table 4 and have been assigned as per the designated reference.

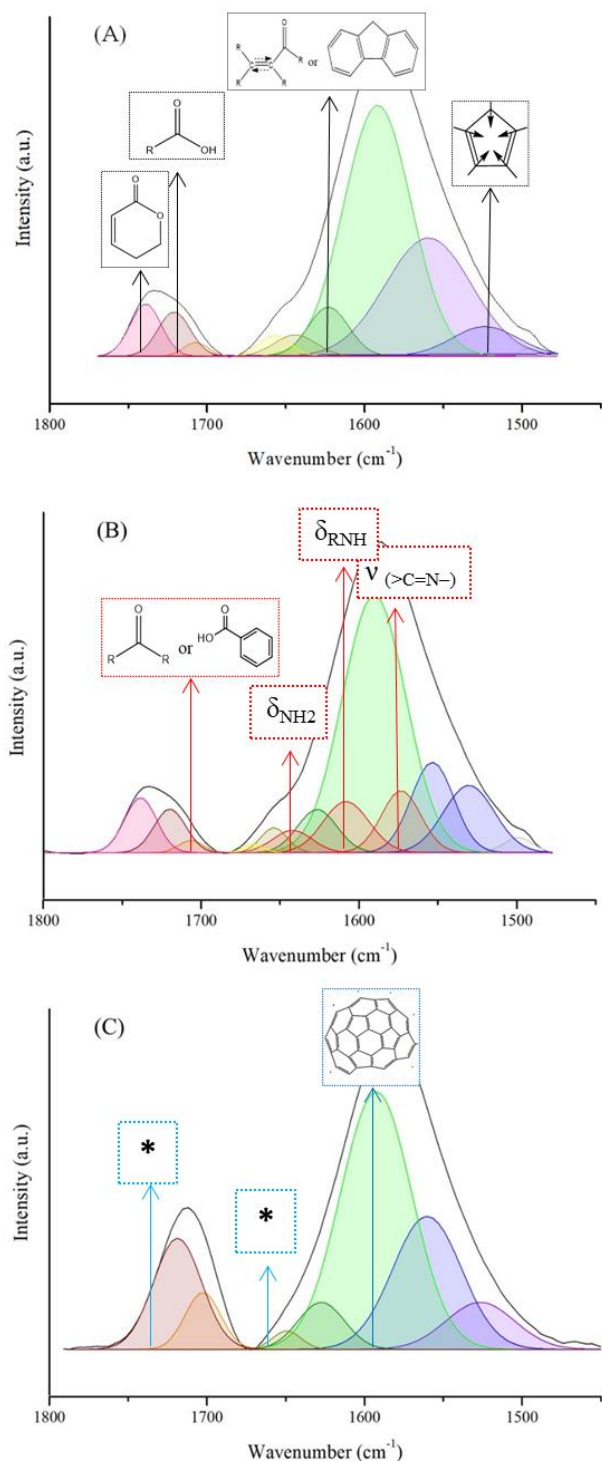
**Table 4.** Deconvolution FTIR spectroscopic bands measured for the ZTC, N-ZTC and P-ZTC samples ( $\nu$  in  $\text{cm}^{-1}$ , A (area) in %).

$\nu$ [ $\text{cm}^{-1}$ ]	Assignment	Vibration type	ZTC		N-ZTC		P-ZTC		$\sigma^+$ ( $\pm$ )	Ref.
			$\nu$	A	$\nu$	A	$\nu$	A		
			[ $\text{cm}^{-1}$ ]	[%]	[ $\text{cm}^{-1}$ ]	[%]	[ $\text{cm}^{-1}$ ]	[%]		
1739		$\nu_{>\text{C}=\text{O}}$	1739	4.44	1739	4.74	–	–	0.20	[32, 37]
1720		$\nu_{>\text{C}=\text{O}}$	1721	3.93	1720	3.96	1718	13.18	1.32	[34-35]
1705		$\nu_{>\text{C}=\text{O}}$	1707	0.94	1707	0.88	1702	4.54	2.71	[14, 32]
1668	$-\text{NH}_2$	$\delta_{\text{NH}_2}$	–	–	1669	0.36	–	–	–	[32, 38]
1656	$-(\text{R})\text{N}-\text{H}$	$\delta_{\text{RNH}}$	–	–	1656	1.77	–	–	–	[32, 38]
1657		$\nu_{>\text{C}=\text{O}}$	1657	1.78	–	–	–	–	–	[32, 34]
1645		$\nu_{>\text{C}=\text{C}<}$	1644	2.43	1643	3.19	1648	1.82	2.40	[32, 34]
1624	PAH	$\nu_{>\text{C}=\text{C}<}$	1623	5.44	1624	8.29	1625	5.94	1.02	[14, 32]
1606	$-(\text{R})\text{N}-\text{H}$ or PAH	$\delta_{\text{RNH}}$ $\nu_{>\text{C}=\text{C}<}$	–	–	1607	6.74	–	–	–	[14, 32]



1591	PAH	$\nu_{(>C=C<)}$	1592	46.43	1590	35.18	1591	40.73	1.48	[14, 32]
1573	$>C=N-$	$\nu_{(>C=N<)}$	-	-	1573	-	-	-	-	[14, 32]
1560	PAH	$\nu_{(>C=C<)}$	1560	27.89	1560	28.83	1561	25.40	0.85	[14, 32]
1524		$C_5$ breathing	1523	5.40	1522	5.63	1526	6.04	1.71	[14, 32]
$R^2$				0.999		0.999		0.999		

---



**Figure 9.** Deconvolution of the FTIR spectra in the region 1800–1450 cm<sup>-1</sup> for the samples ZTC (A), N-ZTC (B) and P-ZTC (C).

As can be seen in Figure 9, the stretching vibration  $>\text{C}=\text{C}<$  gives rise to a strong band with a maximum around 1590 cm<sup>-1</sup>. The position of this band varies to some extent in the three samples as a function of the nature of the substituents on the two carbon atoms. The intensity and frequency of the bands vary depending on the symmetry and conjugation. The peak at

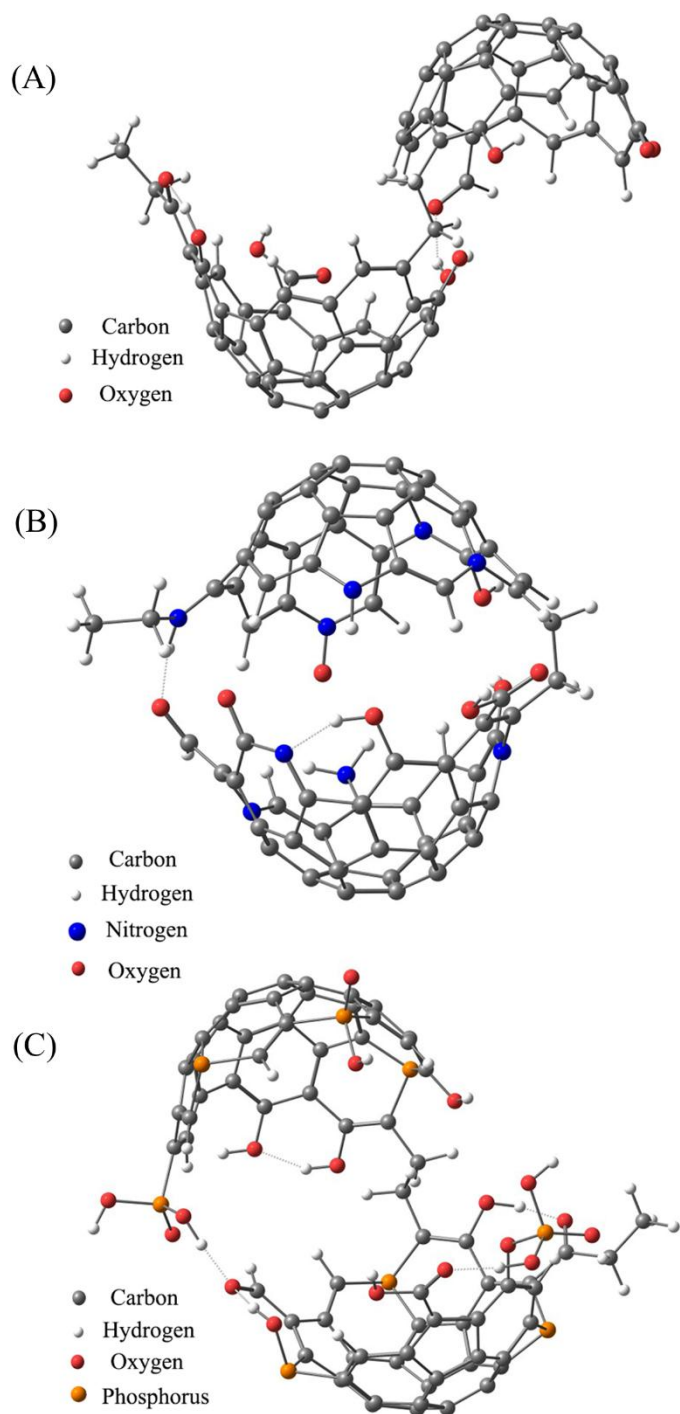
1657  $\text{cm}^{-1}$  represents  $\nu (>\text{C}=\text{C}<)$  stretching vibrations of an isolated  $\text{C}=\text{C}$  double bond or, the non-conjugated one<sup>[14]</sup>. This adsorption band is higher in intensity for the ZTC sample, less abundant in the N-ZTC sample and almost completely absent in the P-ZTC sample; this result is in line with the adsorption band corresponding to the  $\text{C}-\text{H}$  group at 3043  $\text{cm}^{-1}$ . Another interpretation of this band is the  $\nu (>\text{C}=\text{O})$  stretching vibration of the ketone group connected to aliphatic unsaturated double bonds and/or to aromatic rings. Specifically, the common contributions for the three samples identified are: (I) the adsorption band at 1645  $\text{cm}^{-1}$  assigned as  $\nu (>\text{C}=\text{C}<)$  of  $>\text{C}=\text{C}<$   $\text{sp}^2$  atoms conjugated with  $>\text{C}=\text{O}$  or  $>\text{C}=\text{C}<$  groups in a fluorene-like structure; (II) the band at 1591  $\text{cm}^{-1}$  assigned as  $\nu (>\text{C}=\text{C}<)$  in corannulene- or sumanene-like structures; (III) the band at 1560  $\text{cm}^{-1}$  attributed to  $\nu (>\text{C}=\text{C}<)$  stretching vibrations of delocalized conjugated  $>\text{C}=\text{C}<$  double bonds in  $\text{C}_{36}\text{H}_9$  buckyball, and the band at 1524  $\text{cm}^{-1}$  identified as the  $\text{C}_5$  ring breathing.<sup>[32, 34]</sup>

The bands at 1668  $\text{cm}^{-1}$  and 1606  $\text{cm}^{-1}$  in the spectrum of the N-ZTC sample correspond to the  $\text{N}-\text{H}$  bond for the primary ( $\text{RNH}_2$ ) and secondary amines ( $\text{R}_2\text{NH}$ ), respectively.<sup>[32]</sup> The corresponding stretching of this bond (3500–3300  $\text{cm}^{-1}$ ) was not revealed as it was hidden by the intramolecular hydrogen bond bands and by the  $\text{O}-\text{H}$  adsorption band, as already reported.<sup>[39]</sup>

In the construction of the deconvolution model, a band around 1573  $\text{cm}^{-1}$  related to the presence of pyridine-like groups has also been included. This band, as well as those relating to amides, were very difficult to assign due to the overlapping of the  $>\text{C}=\text{C}<$  and  $\text{C}-\text{N}$  and  $\text{C}=\text{N}$  peaks and also to the low ratio between nitrogen atoms and carbon atoms carbon. This overlapping did not allow the observation of the  $\text{C}-\text{N}$  and  $\text{C}=\text{N}$  bands with standard FTIR spectroscopic attribution. However, the corresponding functional groups related to the presence of amide and pyridine-like groups have been inserted in the deconvolution model since the experimental XPS and  $^{15}\text{N}$  NMR results identify their presence.

Considering the standard deviation of the peaks, the deconvolution model in the region between 1800–1450  $\text{cm}^{-1}$  (Table 4) appears to be good, but not self-consistent. For this reason, a further verification by DFT modelling of the three samples ZTC, N-ZTC and P-ZTC at B3LYP/6-311G(d,p) (Figure 10) and B3PW91/6-311G(d,p) levels were carried. The initial S-shaped dimeric buckyball (DBB) structure  $(\text{C}_{36}\text{H}_9)_2(\mu\text{-C}_2\text{H}_4)$  ( $\text{C}_{74}\text{H}_{22}$ ) was based on the Nishihara I model ( $\text{C}_{36}\text{H}_9$  with  $\text{H}/\text{C}$  ratio = 0.25)<sup>[11]</sup> and therefore have a close  $\text{H}/\text{C}$  ratio of 0.30. After introducing the oxygenated functional groups (lactone,  $-\text{COOH}$ ,  $-\text{COH}$  and  $-\text{COEt}$ ) on the basis of XPS, the  $\text{H}/\text{C}$  ratio of the ZTC model ( $\text{C}_{74}\text{H}_{24}\text{O}_{10}$ ) is slightly increased

up to 0.31. In the N-ZTC ( $C_{71}N_9H_{25}O_8$ ) and P-ZTC ( $C_{73}P_8H_{28}O_{18}$ ) models, the H/C ratio is further increased up to 0.35 and 0.38, correspondingly.



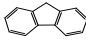
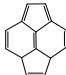
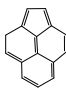


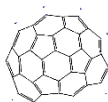
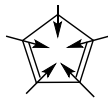
**Figure 10.** B3LYP/6-311G(d,p) optimized geometry of ZTC ( $C_{78}H_{24}O_{10}$ ) (A), N-ZTC ( $C_{71}N_9H_{25}O_8$ ) (B), and P-ZTC ( $C_{73}P_8H_{28}O_{18}$ ) (C) structures.


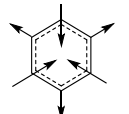
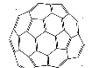
According to the DFT analysis, the  $>C=C<$  stretching vibrations in the frequency range from  $1650\text{ cm}^{-1}$  to  $1560\text{ cm}^{-1}$  are observed (Table 5). At higher frequencies ( $1649\text{--}1639\text{ cm}^{-1}$ ), the  $\nu(>C=C<)$  stretching vibrations are observed in local conjugated domains having the form of fluorene-like structures, then in conjugated pyracene-like and cyclopenta[cd]phenalene-like

structures (at 1634–1600  $\text{cm}^{-1}$ ). These domains increased to corannulene-like and sumanene-like structures (at 1603–1583  $\text{cm}^{-1}$ ), and finally, this vibration movement covers the entire  $\text{C}_{36}\text{H}_9$ -buckybowl structure (1584–1558  $\text{cm}^{-1}$ ).

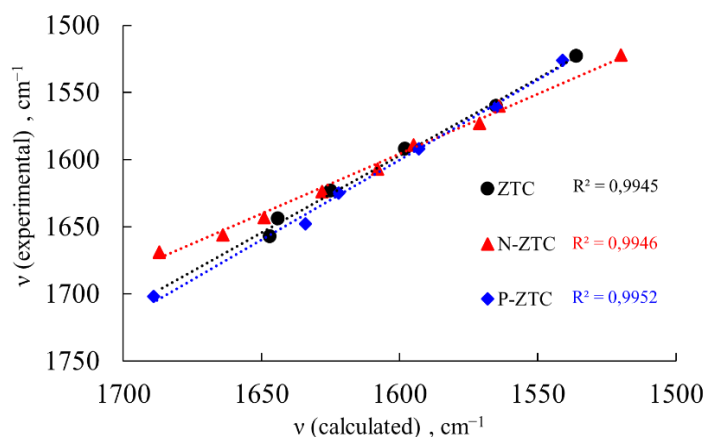
As can be seen from the comparison between the experimental (Table 4) and theoretical data (Table 5 and Table S1) the calculated frequencies differ slightly from the observed frequencies. The difference is attributable to basis set deficiencies or electron correlation effects, or both.

**Table 5.** B3LYP calculated FTIR frequencies ( $\text{cm}^{-1}$ ) and their intensities (in brackets). The values are reported without the use of scaling factors.

Type of vibration	Assignment	DBB- $\text{C}_{36}$ [ $\text{cm}^{-1}$ ]	ZTC [ $\text{cm}^{-1}$ ]	N-ZTC [ $\text{cm}^{-1}$ ]	P-ZTC [ $\text{cm}^{-1}$ ]	
$\nu$ ( $>\text{C}=\text{O}$ )	Lactone		1816(696)	1761(269)		
	–COOH	–	1755(277)	1609(53)	1689(2051)	
	–COH		1692(278)	1602(204)	1607(188)	
	–COEt		1647(351)			
$\delta$ (H–N–H)	– $\text{NH}_2$		–	1687(725)	–	
				1664(82)		
$\nu$ ( $>\text{C}=\text{C}<$ ) in fluorene-like structure			1644(41)	1649(117)	–	
			1639(7)	1645(2)		
$\nu$ ( $>\text{C}=\text{C}<$ ) in pyracene-like structure			1627(2)	1630(19)	1628(32)	
			1622(9)	1625(49)	1626(30)	1622(310)
$\nu$ ( $>\text{C}=\text{C}<$ ) in cyclopenta[cd]phenalene-like structure			1614(39)	1610(53)	1602(66)	
			1606(11)	1608(20)	1608(178)	1600(147)
$\nu$ ( $>\text{C}=\text{C}<$ ) in corannulene-like structure			1604(3)	1607(11)	1595(25)	
			1601(19)	1604(52)	1601(97)	1593(137)
$\nu$ ( $>\text{C}=\text{C}<$ ) in sumanene-like structure			1600(43)	1603(0)	1595(51)	
			1602(6)	1598(87)	1589(25)	1591(91)
$\nu$ ( $>\text{C}=\text{C}<$ ) in $\text{C}_{36}\text{H}_9$ buckybowl structure			1584(29)	1574(50)		
			1575(2)	1582(26)	1571(67)	
			1575(2)	1565(208)	1567(3)	1570(124)
			1558(17)	1560(21)	1564(117)	1565(186)
C5 ring breathing			1556(48)		1560(51)	
			1556(12)	1550(14)	1546(17)	
			1556(15)	1547(69)	1554(8)	1541(99)
			1536(2)	1536(42)	1550(92)	1536(23)
			1524(2)	1510(135)		1535(74)
$\delta$ (R–N–H)	–EtNH		–	1586(106)	–	
				1544(163)		
$\nu$ ( $>\text{C}-\text{N}-$ )	$>\text{C}=\text{N}<$			1538(42)		
	$>\text{C}-\text{N}(\text{HR})$	–	–	1536(7)	–	
	$>\text{C}-\text{NH}_2$			1520(79)		
				1513(36)		
			1475(13)			

$\delta$ OH	-	-	1519(34)	1643(46)	1523(55)
			1455(42)	1465(1)	1457(91)
					1515(44)
				1510(12)	1503(19)
			1507(36)	1509(15)	1501(59)
$\delta$ CH <sub>2</sub>	-CH <sub>2</sub>	1509(3)	1506(76)	1508(134)	1498(16)
		1495(7)	1501(361)	1503(7)	1492(9)
		1477(19)	1493(280)	1490(19)	1484(28)
				1470(31)	1481(25)
					1452(36)
$\nu$ (Kekule)		1499(16)	1488(43)	1499(112)	1506(434)
C6 ring breathing		1489(22)	1487(9)	1497(17)	1477(20)
		1481(50)	1480(64)	1480(18)	1472(152)
		1480(255)	1474(255)	1466(56)	1465(109)
			1439(48)		
$\nu$ (David star)		1437(33)	1437(17)	1441(14)	1441(121)
		1427(13)	1430(52)	1438(126)	1438(110)
		1411(2)	1429(34)	1428(142)	1423(121)
			1377(61)	1427(18)	1419(42)
$\nu$ (P=O)	-O(HO) <sub>2</sub> P=O				1322(358)
	-(HO) <sub>2</sub> P=O	-	-	-	1253(391)
	-(HO)P=O				1242(68)
$\nu$ (N-O)	-	-	-	1312(43)	-
$\nu$ (C-C)(=C)	(C)CH <sub>2</sub> CH <sub>2</sub> -(C)	1175(1)	1153(69)	1159(54)	1096(8)
		1130(18)	1135(21)	1132(60)	1076(69)
			1133(25)	1115(30)	
		1117(11)		1081(40)	
Rings breathing in C <sub>36</sub> H <sub>9</sub>		1118(1)	1121(76)		1059(156)
buckybowl structure		1049(5)	1114(294)	1064(16)	1057(45)
		1046(3)	1106(59)	1058(10)	1047(21)
				1049(16)	
				1168(96)	
$\nu$ (C)-C-C-(C)	(C)CH <sub>2</sub> -CH <sub>2</sub> (C)	1034(5)	1026(32)	1159(54)	975(4)
				1036(62)	
					1042(7)
$\delta$ (P-O)	-	-	-	-	1031(38)
					1022(23)
					1006(3)
					851(173)
$\nu$ (P-OH)	-	-	-	-	839(297)
					826(45)

As a verification method, a linear relationship method is applied to determine the origin of the peak position with respect to the theoretically calculated one (Figure 11 and Figure S7). The larger the correlation coefficient ( $R^2$ ), the greater the correlation between the observed frequencies and the calculated frequencies is found.



**Figure 11.** Linear relationship between the observed peak positions and the B3LYP/6-311G(d,p) calculated wavenumbers of different complexes in the IR spectral region of 1740–1500  $\text{cm}^{-1}$  for samples ZTC, N-ZTC and P-ZTC.

A good correlation between the observed peak positions and the calculated ones by B3LYP/6-311G(d,p) ( $R^2 = 0.994$  for ZTC, 0.995 for N-ZTC and 0.995 for P-ZTC) and B3PW91/6-311G(d,p) ( $R^2 = 0.983$  for ZTC, 0.996 for N-ZTC and 0.993 for P-ZTC) are found (Figure 11 and Figure S8). The linear correlation provides further evidence that the deconvolution study is reliable. The linear fitting between the experimental results and the B3LYP/6-311G(d,p) model also demonstrates that the deconvolution model, based on the FTIR spectroscopy study itself and the conjugated analysis of other characterization techniques such as NMR and XPS, enables a reliable characterization of nitrogen in the FTIR spectrum. The difference between the theoretical and experimental models shows a linear trend with an  $R^2$  equal to 0.995 for the N-ZTC sample. In the calculation of this trend, not only were the 6 points relating to the possible stretching of the  $\text{sp}^2$  hybridized carbon included, but also those related to the stretching of the  $>\text{C}=\text{N}$ - (pyridine like) and bending of the C–N and N–H groups. In fact, the experimental deconvolution model constructed with the presence of all functional groups with nitrogen has a better linear fit with the presence of the three amide and pyridine-like functional groups than the model without any nitrogen group ( $R^2 = 0.891$ ), or with the sole presence of primary and secondary amides ( $R^2 = 0.948$ ). The presence of this functional group had been revealed by NMR and XPS, but it was challenging to characterize this specific sample using simple FTIR spectrophotometry due to the abundance of peaks located at about  $1590 \text{ cm}^{-1}$  and  $1560 \text{ cm}^{-1}$ .

Generally, the interpretation of the FTIR spectrum of the carbonaceous structures in the  $1300$ – $800 \text{ cm}^{-1}$  region (Figure 8(c)) can be complex as the positions of the bands are not assigned

with satisfactory precision due to their overlapping. However, a comparison of the data allowed better understanding of the impact of each peak on the different functional groups. Generally, in all three samples, it is possible to distinguish a broad band at approximately 1270–1160  $\text{cm}^{-1}$ , expected to be due to the overlapping of the C–O–C and C–O stretching modes of CO bonds and epoxy functional groups.<sup>[40]</sup> In particular, the 1265  $\text{cm}^{-1}$  and 1160  $\text{cm}^{-1}$  vibration modes were attributed to the C–O stretch of ether and epoxide groups on edge sites<sup>[18]</sup>, while the bands located in the region 890–750  $\text{cm}^{-1}$  could be attributed to the C–H out-of-plane bending vibration of the C  $\text{sp}^2$  structure.<sup>[16]</sup> By analyzing the 1300–800  $\text{cm}^{-1}$  region, it is possible to confirm the introduction of phosphorus atoms in the carbonaceous structure of the ZTC. Their presence is confirmed by the observation of bands at 1231, 1200 and 1053  $\text{cm}^{-1}$  for the P-ZTC samples, assigned to the P=O, the P–O and P–O–C stretching vibration, respectively.<sup>[41]</sup>

### 3. Conclusions

In this work, we successfully synthesized ZTC and its N- and P-doped analogues using FAU (Si/Al ratio = 2.1) as the zeolite template and furfuryl alcohol as the carbon precursor. We confirmed the N and P doping of the ZTC by XPS and NMR spectroscopies. Subsequently, we obtained clear FTIR spectra of the ZTC materials by varying the ratio of ZTC to KBr and controlling the humidity. These experimental conditions allowed for a clear analysis of the black ZTC samples. Our results revealed two main types of nitrogen species, namely amide (primary and secondary) and pyridine-like, while P was mainly incorporated as triphenylphosphine oxide and phosphonic acid. To verify the reliability of our results, we employed DFT modeling, calculated at B3LYP/6-311G(d,p) and B3PW91/6-311G(d,p) theoretical levels. The DFT model for the N- and P-ZTC samples, based on the dimeric  $(\text{C}_{36}\text{H}_9)_2(\mu\text{-C}_2\text{H}_4)$  ( $\text{C}_{74}\text{H}_{22}$ ) buckyball structure using experimental XPS, NMR, and FTIR data was developed. Notably, a high correlation was observed between the positions of the observed peaks and the frequencies calculated by B3LYP/6-311G(d,p) ( $R^2 = 0.994$  for ZTC, 0.994 for N-ZTC, and 0.995 for P-ZTC), providing strong evidence for the reliability of the deconvolution study.



## 4. Experimental section/methods

### 4.1. Preparation of zeolitic template

Micron-sized FAU type zeolite (Si/Al ratio = 2.1) for further use as a zeolitic template was prepared according to the previously reported protocol.<sup>[42]</sup> In a typical synthesis, a clear suspension with the molar ratio of 8 Na<sub>2</sub>O : 1 Al<sub>2</sub>O<sub>3</sub> : 10 SiO<sub>2</sub> : 400 H<sub>2</sub>O was prepared and aged at ambient conditions for 24 h without agitation, and then subjected to crystallization in a 250 ml PP bottle at 100 °C for 12 h. The powder was recovered by centrifugation followed by several washing steps with Milli-Q® water until pH = 7.

A part of the FAU sample was ion-exchanged with nitrogen. 3g of FAU was immersed in a 0.1 M NH<sub>4</sub>Cl solution with a ratio of 100 ml/g. The mixture was then heated at 60 °C and stirred for 3 x 30 min. The NH<sub>4</sub>-exchanged FAU (NH<sub>4</sub>-FAU) was collected by centrifugation and dried in an oven at 80 °C overnight. A part of the parent FAU sample was also doped with phosphorous. 3 g of FAU was immersed in a 0.1M Na<sub>3</sub>PO<sub>4</sub> solution with a ratio of 100 ml/g. The mixture was stirred for 3 x 30 min. The PO<sub>4</sub><sup>3-</sup> impregnated FAU (PO<sub>4</sub>-FAU) was collected by centrifugation, dried in an oven at 80 °C overnight, and labeled as PO<sub>4</sub>-FAU.

### 4.2 Preparation of ZTC, N-ZTC and P-ZTC

The synthesis process of ZTC, N-ZTC and P-ZTC includes three stages: carbon precursor impregnation (I), calcination (II), and template dissolution (III) (Figure 1). At stage I, typically, 5 g of FAU zeolite was dehydrated at 300 °C for 3 h and then placed in a glass tube with the sand core connected to a flask containing furfuryl alcohol (FA). Then the whole system was kept in a vacuum and the flask was heated at 100 °C to generate FA vapor. After the FA vapor passed through and adsorbed in the zeolite, the system was restored to a N<sub>2</sub> atmosphere and kept for 24 h. Then the sample was washed with mesitylene to remove FA adsorbed on the external surface followed by a heating at 80 °C for 12 h to remove excess of mesitylene. Then at stage II, the FA-loaded zeolite was heated at 150 °C for 8 h under nitrogen to pre-polymerize the FA. The pre-polymerized sample was heated at 900 °C for 4 h with a heating rate of 5 °C/min under a N<sub>2</sub> atmosphere. Finally, at stage III, the calcinated samples were washed with a 100 mL solution of HF/HCl (0.4 M/0.2 M) and Milli-Q® water and dried at 100 °C overnight. The samples labeled as N-ZTC, and P-ZTC were obtained by the same procedure described above using samples NH<sub>4</sub>-FAU or PO<sub>4</sub>-FAU, correspondingly as precursors.

### 4.3 Characterization

The morphology and crystal size of the samples were characterized using a JEOL SEM-7900F scanning electron microscope (SEM) with an acceleration voltage of 5 kV. Energy dispersive X-ray (EDX) analysis of samples was performed using two Bruker XFLASH 6/30 EDX cameras on the SEM microscope Tescan Mira I LMH under 20 kV. X-ray powder diffraction (XRD) patterns were collected using a Bruker D8 Advance with Cu K $\alpha$  radiation ( $\lambda = 1.5418$  Å). The N<sub>2</sub> physisorption experiments were performed at -196 °C using a Quantachrome Autosorb iQ3 gas-sorption analyzer. The micropore volume was calculated from the v-t plot. The pore size distribution was determined using the Quenched solid density functional theory (QSDFT) method.

#### 4.3.1 Solid-state NMR Spectroscopy

The Magic-angle spinning nuclear magnetic resonance (MAS NMR) spectra of <sup>13</sup>C and <sup>31</sup>P were obtained using a Bruker Avance III-HD 500 MHz (11.7 T) spectrometer with a 4.0 mm outer diameter probe. The resonance frequencies were set at 125.7 MHz and 202.4 MHz for <sup>13</sup>C and <sup>31</sup>P, respectively. The RF nutation frequencies used were 55.6 kHz for <sup>13</sup>C and 20.8 kHz for <sup>31</sup>P, both under a MAS rotation frequency of 12 kHz. A total of 5000-6000 scans were acquired for <sup>13</sup>C, and 420 scans were acquired for <sup>31</sup>P spectra. A recycle delay of 10 s was used for both nuclei. Chemical shifts for <sup>13</sup>C were referenced to the <sup>13</sup>C MAS NMR peak of tetramethylsilane, set at 0 ppm. For <sup>31</sup>P, the chemical shifts were referenced to the <sup>31</sup>P MAS NMR peak of H<sub>3</sub>PO<sub>4</sub>, also set at 0 ppm.

A <sup>15</sup>N cross polarization (CP) MAS NMR spectrum was measured using a Bruker AVANCE III 400 MHz (9.4 T) spectrometer equipped with a 4 mm triple resonance probe at a resonance frequency of 40.5 MHz. The MAS rotation frequency was set at 5 kHz. The contact time for the <sup>1</sup>H – <sup>15</sup>N CP/MAS experiment was 3 ms, and 20000 scans were acquired with a recycle delay of 5s. The <sup>15</sup>N chemical shifts were referenced to the <sup>1</sup>H – <sup>15</sup>N CP/MAS peak of <sup>15</sup>NH<sub>4</sub>Cl acquired at a MAS rate of 5 kHz, which was set at -341.17 ppm (with respect to CH<sub>3</sub>NO<sub>2</sub> at 0 ppm).<sup>[43]</sup> It should be noted that while IUPAC recommends using CH<sub>3</sub>NO<sub>2</sub> as the primary reference, the use of liquid NH<sub>3</sub> as an external reference is also common in practice. To facilitate comparison with the literature, the chemical shift values referenced by CH<sub>3</sub>NO<sub>2</sub> or NH<sub>3</sub> were interconverted using the equation  $\delta_{\text{iso}}(\text{NH}_3) = \delta_{\text{iso}}(\text{CH}_3\text{NO}_2) + 380.5$  ppm for <sup>15</sup>N.<sup>[44]</sup>

#### 4.3.2 FTIR and Raman Spectroscopy

FTIR spectra were recorded on a Nicolet 6700 Fourier transform IR spectrometer (Thermo Scientific, U.S.A.), equipped with a DTGS detector. The ZTC samples ( $0.1 \text{ mg} \pm 0.03$ ) were mixed with KBr ( $100 \pm 3 \text{ mg}$ ) and pressed using 20 mm pellet dies at 6 ton using Specac manual hydraulic press, then placed into and initially pre-treated cell at  $65 \text{ }^\circ\text{C}$  for 320 min to eliminate the adsorbed water (Figure S1 and S2) as reported in the paragraph S.1. FTIR spectra were acquired at room temperature in the mid-infrared region (M.I.R.:  $4000 - 400 \text{ cm}^{-1}$ ), with an optical resolution of  $4 \text{ cm}^{-1}$ , with 128 scans. Raman spectra were obtained using a LabRam HR Evolution Horiba Scientific micro-spectrometer, with laser wavelength of 532 nm in the range of  $4000 - 100 \text{ cm}^{-1}$ . Data processing was performed using LabSpec6 software.

To ensure consistency of the obtained data, FTIR and Raman spectra were post-processed using a “Peakfit” software evaluation. First, the spectra of the dehydrated samples were imported within the Peakfit and interpolated using a cubic spline without smoothing the data. Then, a spline baseline, taken at known zero adsorption positions, was subtracted in the  $1800 - 1470 \text{ cm}^{-1}$  range. FTIR spectra of carbon-related materials present quite complex features and therefore, the spectra were deconvoluted using Gaussian functions to simplify the interpretation and obtain a better understanding and an indicative semi-quantitative analysis of the functional groups presents at the specific wavenumber present in this region. To ensure consistency of the obtained data, peak positions were constrained at specific wavenumbers, while the amplitudes and widths were constrained with a lower bound of 0. Subsequently, the software autonomously centered the Gaussians based on wavenumber, amplitudes, and widths to fit the spectrum trend in this region accurately, using the appropriate number of functions.

#### 4.3.3 DFT calculations

The Nishiahara I structural model of ZTC ( $\text{C}_{36}\text{H}_9$  with H/C ratio = 0.25)<sup>[11]</sup> was used for the DFT simulations due to the highest similarities with experimental results.<sup>[12]</sup> For this purpose, the buckminsterfullerene ( $\text{C}_{60}$ ) structure was spited in half and each buckybowll ( $\text{C}_{30}$ ) was extended to  $\text{C}_{36}$  atoms to fit with Nishiahara I model.<sup>[11]</sup> Then the edge carbon atoms were saturated with hydrogen atoms and  $\text{CH}_2\text{CH}_2$  spacer link was added between the obtained  $\text{C}_{36}\text{H}_9$  buckybowlls. As a result, a S-shaped dimeric buckybowll (DBB) structure  $(\text{C}_{36}\text{H}_9)_2(\mu\text{-C}_2\text{H}_4)$  ( $\text{C}_{74}\text{H}_{22}$  with H/C ratio = 0.30) was obtained. Then in order to model the ZTC structure, the oxygenated functional groups (lactone,  $-\text{COOH}$ ,  $-\text{COH}$  and  $-\text{COEt}$ ) were added in accordance with XPS analysis data. The obtained ZTC structure was described with the following formula  $\text{C}_{78}\text{H}_{24}\text{O}_{10}$  (H/C ratio = 0.31). In the structural models of the N- and P-

doped samples, the compositions were readjusted based on the XPS results as follow: N-ZTC ( $C_{71}N_9H_{25}O_8$  with H/C ratio = 0.35) and P-ZTC ( $C_{73}P_8H_{28}O_{18}$  with H/C ratio = 0.35).

Previously it was shown that calculations at B3LYP/6-311G(d,p) level of theory perfectly reproduce all experimental bond distances and bond angles of bowl-shaped polycyclic aromatic hydrocarbons (such as corannulene).<sup>[45]</sup> It was also shown that this method is the most cost-efficient choice for the qualitative prediction of both FTIR intensities and vibration frequencies of the organic aromatic compounds.<sup>[46]</sup> Calculation at B3PW91/6-311G(d,p) level of theory have a good performance and provide a reliable results in simulating experimental FTIR spectra of organic aromatic compounds.<sup>[47]</sup>

Full geometry optimizations of the structures were carried out with the Gaussian09 (Revision D.01)<sup>[48]</sup> package using the B3LYP<sup>[49]</sup> and B3PW91<sup>[50]</sup> functionals with 6-311G(d,p)<sup>[51]</sup> set without symmetry constraints and with ultrafine integration grid and very tight Self-Consistent Field (SCF) option to improve the accuracy of the optimization procedure. Frequency calculations were performed for all optimized complexes in the gas phase and reported without the use of scaling factors. The nature of all the stationary points on the potential energy surfaces were confirmed by the vibrational analysis. The optimized geometries were visualized using Chemcraft 1.8 program.<sup>[52]</sup>

## Supporting Information

Supporting Information is available from the Wiley Online Library or from the author.

## Acknowledgements

This project has received funding by the Label of Excellence for the Centre of Zeolites and Nanoporous Materials by the Region of Normandy and by the National Key Research and Development Program of China of Ministry of Science and Technology (2022YFE0116000), National Natural Science Foundation of China (No. 22175200, No. 21975285)

The authors wish to thank Ling Wei from Advanced Chemical Engineering and Energy Materials Research Center of China University of Petroleum for the  $^{15}N$  CP-NMR characterization, and Edwin Clatworthy for editing of the manuscript

## References

- [1] a) H. Nishihara, T. Kyotani, *Chem Commun (Camb)* **2018**, 54 (45), 5648, <https://doi.org/10.1039/c8cc01932k>; b) T. Aumond, A. Le Person, I. Batonneau-Gener, H. Vezin, A. Sachse, A. Moissette, *J. Phys. Chem. Lett. C* **2023**, 127 (7), 3486, <https://doi.org/10.1021/acs.jpcc.2c08810>.
- [2] H. Itoi, H. Nishihara, T. Kogure, T. Kyotani, *J. Am. Chem. Soc.* **2011**, 133 (5), 1165, <https://doi.org/10.1021/ja108315p>.
- [3] W. Cao, Y. Huang, D. Li, W. Chen, Z. Qie, X. Pi, Q. Du, X. Lai, Y. Li, *Journal of the Energy Institute* **2023**, 106, 101159, <https://doi.org/https://doi.org/10.1016/j.joei.2022.101159>.
- [4] H. Tanaka, T. Seto, H. Nishihara, T. Kyotani, M. T. Miyahara, *TANSO* **2018**, 2018 (285), 197, <https://doi.org/10.7209/tanso.2018.197>.
- [5] H. Nishihara, P.-X. Hou, L.-X. Li, M. Ito, M. Uchiyama, T. Kaburagi, A. Ikura, J. Katamura, T. Kawarada, K. Mizuuchi, T. Kyotani, *J. Phys. Chem. Lett. C* **2009**, 8 (113), 3189, <https://doi.org/10.1021/jp808890x>.
- [6] R. J. Dubey, J. Nussli, L. Piveteau, K. V. Kravchyk, M. D. Rossell, M. Campanini, R. Erni, M. V. Kovalenko, N. P. Stadie, *ACS Appl. Mater. Inter.* **2019**, 11 (19), 17686, <https://doi.org/10.1021/acsami.9b03886>.
- [7] W. Choi, R. K. Bera, S. W. Han, H. Park, T. W. Go, M. Choi, R. Ryoo, J. Y. Park, *Carbon* **2022**, 193, 42, <https://doi.org/10.1016/j.carbon.2022.02.056>.
- [8] F. J. Isidro-Ortega, J. H. Pacheco-Sánchez, A. González-Ruíz, R. Alejo, *Intern. J. Hydrogen Energy* **2020**, 45 (38), 19505, <https://doi.org/https://doi.org/10.1016/j.ijhydene.2020.05.017>.
- [9] Y. Liu, J. Wang, T. Wang, W.-P. Pan, *Sep. Purif. Technol.* **2022**, 294, <https://doi.org/10.1016/j.seppur.2022.121228>.
- [10] T. Roussel, A. Didion, R. J. M. Pellenq, R. Gadiou, C. Bichara, C. Vix-Guterl, *J. Phys. Chem. Lett. C* **2007**, 111 (43), 15863, <https://doi.org/10.1021/jp0746906>.
- [11] H. Nishihara, Q.-H. Yang, P.-X. Hou, M. Unno, S. Yamauchi, R. Saito, J. I. Paredes, A. Martínez-Alonso, J. M. D. Tascón, Y. Sato, M. Terauchi, T. Kyotani, *Carbon* **2009**, 47 (5), 1220, <https://doi.org/10.1016/j.carbon.2008.12.040>.
- [12] E. E. Taylor, K. Garman, N. P. Stadie, *Chem. Mater.* **2020**, 32 (7), 2742, <https://doi.org/10.1021/acs.chemmater.0c00535>.
- [13] H. Nishihara, H. Fujimoto, H. Itoi, K. Nomura, H. Tanaka, M. T. Miyahara, P. A. Bonnaud, R. Miura, A. Suzuki, N. Miyamoto, N. Hatakeyama, A. Miyamoto, K. Ikeda, T. Otomo, T. Kyotani, *Carbon* **2018**, 129, 854, <https://doi.org/10.1016/j.carbon.2017.12.055>.
- [14] V. Țucureanu, A. Matei, A. M. Avram, *Crit. Rev. Anal. Chem.* **2016**, 46 (6), 502, <https://doi.org/10.1080/10408347.2016.1157013>.
- [15] L. Xin, J. Hu, Y. Xiang, C. Li, L. Fu, Q. Li, X. Wei, **2021**, 14 (10), 2643.
- [16] A. Lazzarini, A. Piovano, R. Pellegrini, G. Leofanti, G. Agostini, S. Rudić, M. R. Chierotti, R. Gobetto, A. Battiato, G. Spoto, A. Zecchina, C. Lamberti, E. Groppo, *Cat. Sci. & Tech.* **2016**, 6 (13), 4910, <https://doi.org/10.1039/C6CY00159A>.
- [17] J. Zhou, W. Li, Z. S. Zhang, X. Z. Wu, W. Xing, S. P. Zhuo, *Electrochim. Acta* **2013**, 89, 763, <https://doi.org/10.1016/j.electacta.2012.11.068>.
- [18] M. Vujković, D. Bajuk-Bogdanović, L. Matović, M. Stojmenović, S. Mentus, *Carbon* **2018**, 138, 369, <https://doi.org/10.1016/j.carbon.2018.07.053>.
- [19] F. Su, X. S. Zhao, L. Lv, Z. Zhou, *Carbon* **2004**, 42 (14), 2821, <https://doi.org/10.1016/j.carbon.2004.06.028>.
- [20] C. Wang, C. Yan, J. Yao, L. Zhang, N. Xu, X. Liu, *J. Porous Mater.* **2008**, 16 (6), 699, <https://doi.org/10.1007/s10934-008-9251-6>.
- [21] a) Y. Zhu, K. Miyake, Y. Shu, K. Moroto, Y. Hirota, Y. Uchida, S. Tanaka, T. Zheng, M.

- Katayama, Y. Inada, E. Morallón, D. Cazorla-Amorós, C. Y. Kong, N. Nishiyama, *Mater. Today Chem.* **2021**, *20*, <https://doi.org/10.1016/j.mtchem.2020.100410>; b) S. Choi, H. Kim, S. Lee, Y. Wang, C. Ercan, R. Othman, M. Choi, *Chem. Eng. J.* **2015**, *280*, 597, <https://doi.org/10.1016/j.cej.2015.06.055>; c) H. Lu, K. Kim, Y. Kwon, X. Sun, R. Ryoo, X. S. Zhao, *J. Mater. Chem. A* **2018**, *6* (22), 10388, <https://doi.org/10.1039/c8ta00850g>.
- [22] R. J. Konwar, M. De, *Micropor. Mesopor. Mat.* **2013**, *175*, 16, <https://doi.org/10.1016/j.micromeso.2013.03.014>.
- [23] L. G. Guex, B. Sacchi, K. F. Peuvot, R. L. Andersson, A. M. Pourrahimi, V. Strom, S. Farris, R. T. Olsson, *Nanoscale* **2017**, *9* (27), 9562, <https://doi.org/10.1039/c7nr02943h>.
- [24] N. A. Kumar, H. Nolan, N. McEvoy, E. Rezvani, R. L. Doyle, M. E. G. Lyons, G. S. Duesberg, *J. Mater. Chem. A* **2013**, *1* (14), <https://doi.org/10.1039/c3ta10337d>.
- [25] J. Liu, H. Liu, Y. Zhang, R. Li, G. Liang, M. Gauthier, X. Sun, *Carbon* **2011**, *49* (15), 5014-5021 <https://doi.org/10.1016/j.carbon.2011.07.018>.
- [26] P. Duan, B. Zhi, L. Coburn, C. L. Haynes, K. Schmidt-Rohr, *Magn. Reson. Chem.* **2020**, *58* (11), 1130, <https://doi.org/10.1002/mrc.4985>.
- [27] A. R. MacIntosh, G. Jiang, P. Zamani, Z. Song, A. Riese, K. J. Harris, X. Fu, Z. Chen, X. Sun, G. R. Goward, *J. Phys. Chem. Lett. C* **2018**, *122* (12), 6593, <https://doi.org/10.1021/acs.jpcc.7b11671>.
- [28] T. Gutmann, E. Bonnefille, H. Breitzke, P.-J. Debouttière, K. Philippot, R. Poteau, G. Buntkowsky, B. Chaudret, *Phys. Chem. Chem. Phys.* **2013**, *15* (40), 17383, <https://doi.org/10.1039/C3CP52927D>.
- [29] X. Guo, X. Xu, X. Xue, X. Li, *Fuel* **2022**, *312*, 122980, <https://doi.org/10.1016/j.fuel.2021.122980>.
- [30] M. Ayiania, E. Weiss-Hortala, M. Smith, J.-S. McEwen, M. Garcia-Perez, *Carbon* **2020**, *167*, 559, <https://doi.org/10.1016/j.carbon.2020.05.055>.
- [31] F. Tuinstra, J. L. Koenig, *J. Chem. Phys.* **1970**, *53* (3), 1126, <https://doi.org/10.1063/1.1674108> %
- [32] S. K. Jha, I. Vasiliev, *J. Phys. Chem. Lett. C* **2018**, *122* (43), 24996, <https://doi.org/10.1021/acs.jpcc.8b06274>.
- [33] L. J. Bellamy, *The Infra-red Spectra of Complex Molecules*, Springer Science & Business Media, **2013**.
- [34] R. Lu, W. Gan, B.-h. Wu, Z. Zhang, Y. Guo, H.-f. Wang, *J. Phys. Chem. B* **2005**, *109* (29), 14118, <https://doi.org/10.1021/jp051565q>.
- [35] J. M. O'Reilly, R. A. Mosher, *Carbon* **1983**, *21* (1), 47, [https://doi.org/10.1016/0008-6223\(83\)90155-0](https://doi.org/10.1016/0008-6223(83)90155-0).
- [36] A. Barroso-Bogeat, M. Alexandre-Franco, C. Fernández-González, V. Gómez-Serrano, *Energy & Fuels* **2014**, *28* (6), 4096, <https://doi.org/10.1021/ef5004733>.
- [37] M. Nishimoto, Y. Uetake, Y. Yakiyama, F. Ishiwari, A. Saeki, H. Sakurai, *J. Org. Chem.* **2022**, *87* (5), 2508, <https://doi.org/10.1021/acs.joc.1c02416>.
- [38] S. Abraham, G. Aruldhas, *Spectrochimica Acta Part A: Molecular and Biomolecular Spectroscopy* **1995**, *51* (1), 79, [https://doi.org/10.1016/0584-8539\(94\)E0076-M](https://doi.org/10.1016/0584-8539(94)E0076-M).
- [39] L. Ghazi Moradi, M. Ganjaee Sari, B. Ramezanzadeh, *Prog. Org. Coat.* **2020**, *142*, 105573, <https://doi.org/10.1016/j.porgcoat.2020.105573>.
- [40] M.-W. Jung, K.-H. Ahn, Y. Lee, K.-P. Kim, J.-S. Rhee, J. Tae Park, K.-J. Paeng, *Microchem. J.* **2001**, *70* (2), 123, [https://doi.org/10.1016/S0026-265X\(01\)00109-6](https://doi.org/10.1016/S0026-265X(01)00109-6).
- [41] J. Qu, W. C. Barnhill, H. Luo, H. M. Meyer, 3rd, D. N. Leonard, A. K. Landauer, B. Kheireddin, H. Gao, B. L. Papke, S. Dai, *Adv. Mater.* **2015**, *27* (32), 4767, <https://doi.org/10.1002/adma.201502037>.
- [42] H. Awala, J. P. Gilson, R. Retoux, P. Boullay, J. M. Goupil, V. Valtchev, S. Mintova, *Nat Mater* **2015**, *14* (4), 447, <https://doi.org/10.1038/nmat4173>.

- [43] P. Bertani, J. Raya, B. Bechinger, *Solid State Nucl. Magn. Reson.* **2014**, 61-62, 15, <https://doi.org/https://doi.org/10.1016/j.ssnmr.2014.03.003>.
- [44] G. Kim, J. Lee, T. Liu, C. P. Grey, *J. Phys. Chem. Lett. C* **2021**, 125 (19), 10558, <https://doi.org/10.1021/acs.jpcc.1c02669>.
- [45] M. A. Petrukhina, K. W. Andreini, J. Mack, L. T. Scott, *J. Org. Chem.* **2005**, 70 (14), 5713, <https://doi.org/10.1021/jo050233e>.
- [46] S. A. Katsyuba, E. E. Zvereva, T. I. Burganov, *J. Phys. Chem. Lett. A* **2013**, 117 (30), 6664, <https://doi.org/10.1021/jp404574m>.
- [47] D. Avcı, S. Bahçeli, Ö. Tamer, Y. Atalay, **2015**, 93 (10), 1147, <https://doi.org/10.1139/cjc-2015-0176>.
- [48] M. J. Frisch, G. W. Trucks, H. B. Schlegel, G. E. Scuseria, M. A. Robb, J. R. Cheeseman, G. Scalmani, V. Barone, G. A. Petersson, H. Nakatsuji, X. Li, M. Caricato, A. V. Marenich, J. Bloino, B. G. Janesko, R. Gomperts, B. Mennucci, H. P. Hratchian, J. V. Ortiz, A. F. Izmaylov, J. L. Sonnenberg, Williams, F. Ding, F. Lipparini, F. Egidi, J. Goings, B. Peng, A. Petrone, T. Henderson, D. Ranasinghe, V. G. Zakrzewski, J. Gao, N. Rega, G. Zheng, W. Liang, M. Hada, M. Ehara, K. Toyota, R. Fukuda, J. Hasegawa, M. Ishida, T. Nakajima, Y. Honda, O. Kitao, H. Nakai, T. Vreven, K. Throssell, J. A. Montgomery Jr., J. E. Peralta, F. Ogliaro, M. J. Bearpark, J. J. Heyd, E. N. Brothers, K. N. Kudin, V. N. Staroverov, T. A. Keith, R. Kobayashi, J. Normand, K. Raghavachari, A. P. Rendell, J. C. Burant, S. S. Iyengar, J. Tomasi, M. Cossi, J. M. Millam, M. Klene, C. Adamo, R. Cammi, J. W. Ochterski, R. L. Martin, K. Morokuma, O. Farkas, J. B. Foresman, D. J. Fox, Gaussian 09 Rev. D.01. Wallingford, CT, **2009**.
- [49] P. J. Stephens, F. J. Devlin, C. F. Chabalowski, M. J. Frisch, *J. Phys. Chem.* **1994**, 98 (45), 11623, <https://doi.org/10.1021/j100096a001>.
- [50] A. D. Becke, M. R. Roussel, *Phys. Rev. A* **1989**, 39 (8), 3761, <https://doi.org/10.1103/PhysRevA.39.3761>.
- [51] A. D. McLean, G. S. Chandler, *J. Chem. Phys.* **1980**, 72 (10), 5639, <https://doi.org/10.1063/1.438980> %
- [52] G. A. Adrienko, Chemcraft. 1.8 (Build 530) ed.; **2017**.